Electric Power Systems Research 218 (2023) 109213

Contents lists available at ScienceDirect

Electric Power Systems Research

journal homepage: www.elsevier.com/locate/epsr

Statistical relationship between RMS and QP spectra of voltage measurements in the 9–150 kHz range

Alexander Gallarreta [a,*], Igor Fernández [a], Deborah Ritzmann [b], Stefano Lodetti [b], Victor Khokhlov [c], David de la Vega [a], Paul Wright [b], Jan Meyer [c]

[a] University of the Basque Country (UPV/EHU), Bilbao, ES-48013, Spain
[b] National Physical Laboratory, Teddington, TW11 0LW, United Kingdom
[c] Technische Universität Dresden, Dresden, 01062, Germany

ARTICLE INFO

Keywords:
Electromagnetic interference
Measurement techniques
Power quality
Smart grids
Voltage measurement

ABSTRACT

The main objective of this work is to obtain an empirical relationship between the root-mean-square and the quasi-peak spectra of voltage recordings in the electrical grid, based on a statistical analysis of a set of on-field measurements for the CISPR Band A (9–150 kHz). The lack of a relationship between the weighting root-mean-square and quasi-peak detectors implies the impossibility of calculating quasi-peak (QP) spectra from root-mean-square (RMS) measurements. It is of great interest that quasi-peak values can be estimated by simple calculations from RMS values, so that comparison to compatibility levels could be applied.

This work defines an empirical relationship between the statistical variation of instantaneous RMS values over time, the maximum RMS value of these instantaneous values and the QP output. This relationship is described in the form of a simple equation that can be applied to RMS provided by the RM-A method, specifically developed for the CISPR Band A.

A method for the fast assessment of QP values from simple RMS receivers is proposed as a potential application of the numerical RMS-QP relationship. Both the numerical RMS-QP relationship and its application as a simple and fast assessment method are evaluated with disturbances recorded in the low voltage grid.

1. Introduction

Electrical power grids are undergoing major structural changes driven by world-wide decarbonization efforts, which are seeing a rapidly increasing penetration of distributed energy resources and low-emissions technology, often connected to the low-voltage (LV) grid. This includes, amongst others, solar photo-voltaic (PV) power generation, electrical storage, and electric vehicle (EV) charging stations, technologies that interact with the grid via power electronics converters. While underpinning the evolution towards a low-carbon grid, smart grids technologies such as power converters are raising concerns related to their impact on power quality and electromagnetic compatibility (EMC) [1]. Amongst them, conducted emissions in the frequency range from 9 kHz to 150 kHz have been identified as a relevant aspect to be monitored for safeguarding of EMC, especially as the share of converter-connected devices keeps growing [2–5]. The research on the increasing presence of conducted non-intentional emissions (NIE) performed in the last decade led to the identification and classification of several cases of electromagnetic interference (EMI), which have been reported, amongst others, by CENELEC in [6,7]. It has been shown that, in this frequency range, NIE can have detrimental effects including, notably, interference with power line communications (PLC) and degradation of electrical equipment which have been found to suffer from malfunctioning, additional heating and lifetime reduction, and generation of unwanted acoustic noise [8–14]. Prevention of widespread EMI and power quality (PQ) problems requires an adequate EMC framework, which is well established for emissions up to 9 kHz, but it still requires further definition and coordination for frequencies up to 150 kHz. As a representative example, compatibility levels (CL) and immunity limits were defined in the last years in IEC 61,000-2-2 [15] and IEC 61,000-4-19 [16], respectively, but emissions limits for most of the electronic devices remain under discussion.

Another pivotal element of the EMC framework is that no normative method for supraharmonic distortion measurements has been defined, i.e., grid disturbances above 9 kHz. Only the Annex C of IEC 61,000,430 [17] outlines several non-normative methods that are currently under

* Corresponding author.
E-mail address: alexander.gallarreta@ehu.eus (A. Gallarreta).

https://doi.org/10.1016/j.epsr.2023.109213
Received 13 October 2022; Received in revised form 3 February 2023; Accepted 9 February 2023
Available online 14 February 2023

consideration by the IEC SC77A Working Group 9. Therefore, consensus about normative methods in the 9–150 kHz range still needs to be reached.

The authors of this work have identified four desirable characteristics to guide the design of normative grid disturbance measurement methods: i) measurement values should be comparable to compatibility levels in terms of applied bandwidth and type of detector (defined by IEC as devices for discerning the existence or variations of waveforms [18]), ii) measurement values should reflect relevant physical interference phenomena and waveform characteristics, iii) the method should have high reproducibility such that two instruments from different manufacturers provide the same assessment result within accuracy requirements, iv) the method should be computationally light to limit the cost of PQ instruments and to enable implementation on existing platforms.

For the frequency range from 9 kHz to 150 kHz, the measurement method defined in informative Annex B of IEC 61,000-4-7 [19] is under consideration in Annex C of IEC 61,000-4-30. This method provides root-mean-square (RMS) values corresponding to the definition of the CL in the 2–9 kHz range and the method extends the principles of the normative method for harmonics below to 2 kHz, limiting the complexity of its implementation on existing PQ instruments. For the frequency range from 9 kHz to 150 kHz, informative Annex C of IEC 61,000-4-30 considers three options, but only one provides quasi-peak (QP) values which correspond to the definition of CL in this frequency range. This is the method in CISPR 16–1–1 [20], referred to as CISPR 16 method in the rest of this paper.

The CISPR 16 method is normative for emissions assessment of individual equipment under test (EUT) in a laboratory setting with the use of a line impedance stabilization network (LISN). Concerns have been raised about the application of this method for grid measurements for several reasons. Firstly, the CISPR 16 standard defines the method to evaluate QP values by specifying black-box requirements that refer to analogue superheterodyne EMI receivers to scan the frequency range sequentially over long measurement times assuming constant EUT behavior. Assessment of grid disturbance levels requires simultaneous and continuous measurement of the entire frequency range, since power grid disturbances vary over time. The CISPR 16 standard does allow for implementation of digital instruments with the capability to measure the whole frequency range simultaneously [21]. However, to comply with all requirements, a digital QP detector requires a near-continuous evaluation of the signal amplitude in each frequency band, which results in high computational burden compared to evaluation of RMS values, as demonstrated in [22]. Secondly, the black-box approach combined with tolerances up to 2 dB (about +/−25%) allows for different implementation possibilities that comply with CISPR 16 but may not be reproducible to the accuracy of 5–10% typically required for PQ measurement methods [17]. Furthermore, a recent study has found that the wide tolerances allowed by the CISPR 16 standard generate numerous compliant implementations, which provide results with differences of up to 35% for the same input signal [23]. Additionally, RMS values have been demonstrated to be reflective of relevant PQ interfering mechanisms [24,25], while QP values were originally developed to assess emissions primarily to protect radio transmission from interference. Therefore, while QP values are useful to assess disturbances amplitude against CL, there is a question of whether they provide useful information about the quality of power supply.

Due to these limitations, there is a strong incentive to develop an alternative method that provides QP values for comparison with compatibility levels in the frequency range 9150 kHz while also satisfying the other desirable characteristics of reflecting relevant interference phenomena and waveform characteristics, high reproducibility and low computational burden. Several methods have been proposed previously as alternatives to those listed in IEC 61,000,430 Annex C, including methods utilizing wavelet packet decomposition [26], compressive sensing [27–29], phase-locked loop [30], and a subsampling approach [31]. Comparison of such methods can be found in the literature showing that RMS values representative of signal energy can be obtained to varying degrees of accuracy [32–34], however, none provides a QP value that can be compared to compatibility levels up to 150 kHz. This gap was addressed in [22] by proposing the concept of a Light-QP method which evaluates RMS values in a first stage, also known as RM-A method [35], and applies a digital QP detector in the second stage [22].

The definition of a relationship between RMS and QP values would be beneficial for PQ manufacturers, as it would avoid the implementation of a QP detector in PQ instruments, which would provide QP outputs with simpler calculations and less computational resources in cheaper devices. Furthermore, the RMS-QP relationship could be used as a first assessment of CL compliance with existing PQ devices, without the need to start the analysis from the raw sampled values.

This paper investigates and defines the statistical relationship between RMS and CISPR 16 QP values for the 9–150 kHz range, based on correlation analysis of grid signals. This relationship is quantified in the form of a simple equation, which is the basis of a novel method to obtain QP values from RMS measured values. The novel method has the benefits of providing RMS values characteristic of the underlying waveforms and of PQ interference mechanisms, but also QP values linked to CISPR 16 QP through a statistical model to enable a comparison with compatibility levels, with a lower computation burden than a digital CISPR 16 implementation. The proposed numerical relationship RMS-QP, and consequently, the accuracy of the proposed method, are evaluated by comparing the results to the QP values provided by the CISPR 16 method for the same grid signals.

The rest of this article is structured as follows. Firstly, the aim of this work is explained. Secondly, the assessment and measurement of supraharmonic voltage values in the LV grid is described. Then, the empirical statistical relationship QP-RMS spectra developed in this work is described. Based on this empirical relationship, a measurement method developed in this paper is explained. Lastly, the conclusions of this work are given.

2. Approach of the study

This section describes the rationale used in this study for defining the relationship between RMS and QP values. Therefore, this section describes the fundamentals used to obtain the aforementioned relationship, the procedure of computing the RMS amplitudes of the voltage values in the 9–150 kHz region, and the underlying rationale of the statistical study to achieve the RMS-QP relationship.

2.1. Fundamentals of the proposed methodology

The measurement method to obtain QP spectra for 9–150 kHz is described in the CISPR 16–1–1 standard. The QP detector is based on a resistor-capacitor circuit and a critically damped meter that weights the measured voltage values. Due to the performance of this circuitry, the QP is a metric that responds not only to the amplitude of the input values, but also, in case of non-continuous emissions, to the number of occurrences and their duration within the measurement time. Therefore, an impulsive emission of a certain amplitude that is repeated over time provides a QP output of greater amplitude than a single impulsive emission.

This paper includes a statistical study of the RMS amplitude values of non-continuous emissions over time. The study aims to obtain approximate QP values, combining the RMS amplitude of the emissions and their variability over time. For this purpose, the measured RMS values are stored, and the maximum value of this metric after a three second interval is identified. The statistical variation of the RMS amplitude is computed over the same measurement interval. Since the maximum RMS value corresponds to a greater value than the QP for time-varying voltages in the grid [32], the QP values can be estimated by subtracting a

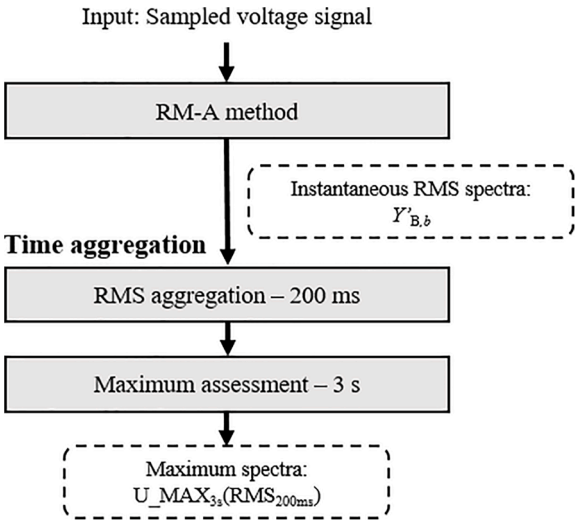

Fig. 1. Schematic overview of the RM-A method and the aggregation of spectral values.

'conversion factor' to the maximum RMS values. For that, the relation between this conversion factor and the RMS amplitude variation over time must be obtained by statistical analysis.

2.2. Assessment of RMS spectra in the CISPR Band A (9–150 kHz)

The proposed method to estimate the QP values is based on an RMS measuring receiver. But there is no normative method for calculating the RMS spectra of voltage values in the 9–150 kHz band. The IEC 61,000–4–30 standard only suggests the measurement method described in Annex B of IEC 61,000–4–7 to quantify the RMS amplitude in the supraharmonic region. This method is based on two main calculation blocks to compute the RMS values of the disturbances propagated through the LV grid. Firstly, the spectral analysis is performed by means of rectangular windows of 200 ms length, which provides frequency components with a resolution bandwidth and a frequency-step-size (separation between adjacent frequency components) of 5 Hz. Secondly, the IEC 61,000–4–7 standard defines a spectral grouping of the outputs of the discrete Fourier transforms (DFT) to obtain the frequency bands, which are the spectral samples after the grouping. This grouping provides a resolution bandwidth of 200 Hz for the frequency bands, which is in line with the resolution bandwidth of the CL regulated in IEC 61,000–2–2 for the 9–150 kHz band. Nevertheless, this method was never considered for the 9–150 kHz band, since it was designed for the 2–9 kHz band. Moreover, the IEC 61,000–4–30 standard does not provide any guidance on how to apply this method to the CISPR Band A (9–150 kHz), so it is assumed that the method should be applied with no modifications.

A recent study has overcome the latter issue proposing an adaptation of the IEC 61,000–4–7 method to the CISPR Band A, which has been labeled as RM-A method [35]. The novel method aims to reduce the computational effort based on IEC 61,000–4–7 proposing two adaptations to quantify the interference mechanisms of LV grid in the 9–150 kHz band. Firstly, a shorter rectangular window of 20 ms length is proposed for a more detailed temporal resolution with respect to the IEC 61,000–4–7 method. And secondly, the frequency components obtained in the Fourier analysis every 50 Hz are proposed to be grouped symmetrically for a more accurate frequency allocation of the 200 Hz bandwidth the frequency components. This technique provides instantaneous RMS spectra ($Y'_{B,b}$ in Fig. 1), with a resolution bandwidth of 200 Hz and 100 Hz of frequency-step-size [35].

2.3. Assessment of the maximum value

In order to compute the maximum values of the spectra for 3 s intervals, the outputs of the RM-A method are aggregated in two steps (see Fig. 1). Firstly, the instantaneous RMS spectra are aggregated by means of the RMS operation in 200 ms measurement intervals. Then, the assessment of maximum spectra (U_MAX$_{3s}$(RMS$_{200ms}$) in Fig. 1) are computed based on the outputs of the previous step in 3 second intervals. These aggregated results are comparable to the maximum values obtained with the extension of the IEC 61,000–4–7 in the CISPR Band A [35].

In this study, the instantaneous RMS spectra and the maximum spectra of the RM-A method are used to relate the RMS spectra with the QP values of an implementation of CISPR 16. Moreover, the statistical comparison of the results of both methods is used to establish an empirical relationship between RMS and QP spectra.

2.4. Statistical analysis

The statistical study aims to relate the maximum RMS values provided by the RM-A method and the QP values from CISPR 16 with respect to a third metric. The third metric is based on characterizing the variability of the RMS voltage values over time with statistical parameters. For this purpose, recordings measured in the LV grid, containing typical waveforms, are used in the analysis. The calculations are performed, for each frequency band, on the instantaneous RMS spectra ($Y'_{B,b}$) provided by the RM-A method, the maximum RMS values (U_MAX$_{3s}$(RMS$_{200ms}$)) and the QP values obtained with the CISPR 16 method.

3. Methodology

This section describes the methodology applied to obtain the empirical relationship between the RMS values (results of the RM-A method [35]) and the QP values (results of the digital implementation of the CISPR 16 method [22]).

3.1. Input signals for the RMS-QP empirical relationship

A set of 59 Vage recordings measured in different scenarios of the LV distribution grids in Spain and Germany were used in this study, 49 of them were measured at the point-of-connection (POC) of PLC-based smart meters and 10 were recorded at the POC of PV inverters and EV chargers.

The recordings performed in Spain were measured with an acquisition system composed of a voltage probe and a digital oscilloscope connected to a laptop that automatizes and stores the raw voltage data. The system provides an amplitude resolution of 16-bits per sample at a sampling rate of 8.92 MHz [3]. The voltage probe includes a band-pass filter with a flat amplitude response for the 10–500 kHz frequency range, and it provides a galvanic isolation to avoid the fundamental and to protect the measurement equipment [36].

For the signals measured in Germany, an analog-to-digital converter with an amplitude resolution of 16-bits and a sampling rate of 1 MHz was used. This measurement system implements, before the transient recorder, an analog Butterworth anti-aliasing filter with a cutoff-frequency of 300 kHz. Additionally, a digital high-pass filter is used to avoid the spectral leakage generated by the mains and low order harmonics [37].

The complete dataset of 59 recordings was divided randomly into two groups. The 'model dataset' contains 30 signals which was used for obtaining the empirical relationship between the RMS and the QP values. The 'validation dataset', composed of 29 recordings, was used to evaluate the accuracy of the obtained empirical relationship.

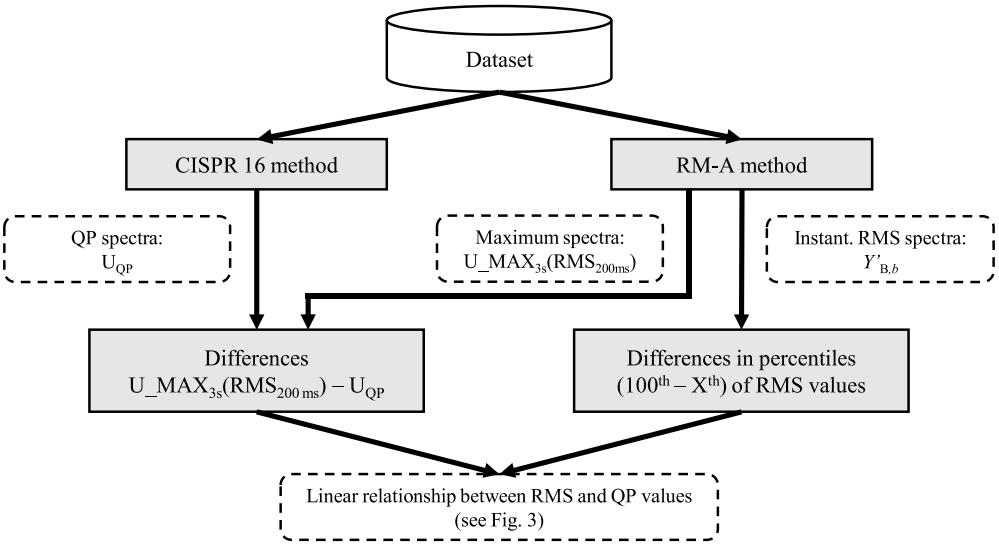

Fig. 2. Schematic overview of the procedure for obtaining the linear relationship between RMS and QP values.

3.2. Empirical relationship between QP and RMS spectra

The main difference between QP and RMS is that QP is a metric designed to incorporate the variation over time of the voltage. Therefore, the variability over time of the RMS values is a key element to establish the relationship between the QP and the maximum RMS. The QP and the maximum of the RMS values are obtained by applying the CISPR 16 method and the RM-A method, respectively, to the measurement recordings, whereas the time variation of the instantaneous RMS values is characterized by its statistical distribution within the aggregation time.

The relevant variables are (see Fig. 1 and Fig. 2):

- U_{QP}: QP values obtained with the CISPR 16 method [22].
- $U\_MAX_{3s}(RMS_{200\ ms})$: maximum values provided by the RM-A method [35].
- $Y'_{B,b}$: instantaneous RMS values, obtained every 20 ms with RM-A method, where *b* represents center frequency of the frequency bands[35].

The analysis was developed for each frequency band of all the 59 recordings used in this analysis. As there are 705 200 Hz frequency bands for each signal in the 9–150 kHz range, a total of 41,595 frequency bands were assessed in the study. This implies 41,595 values of QP and maximum outputs and a total of 6239,250 instantaneous RMS values considered in the analysis.

3.3. Preliminary results

The results of this first analysis, whose procedure is represented in Fig. 2, show that there is a linear relationship between:

- the difference between the maximum values and its corresponding QP ($U\_MAX_{3s}(RMS_{200\ ms}) - U_{QP}$ in Fig. 2), and
- the spread of the instantaneous RMS values during the aggregation time, calculated as the difference between the maximum value and a specific percentile of the distribution over time ($100th - X^{th}$ in Fig. 2). The difference between the maximum value and a specific percentile is an indication of the statistical variability of the signal over the time, as a greater time variability provides greater figures for this difference. Since the recordings are of 3 s length and the RM-A method provides instantaneous RMS values every 20 ms, the statistical analysis of each frequency bands is assessed with 150 instantaneous RMS values for each frequency bands [35].

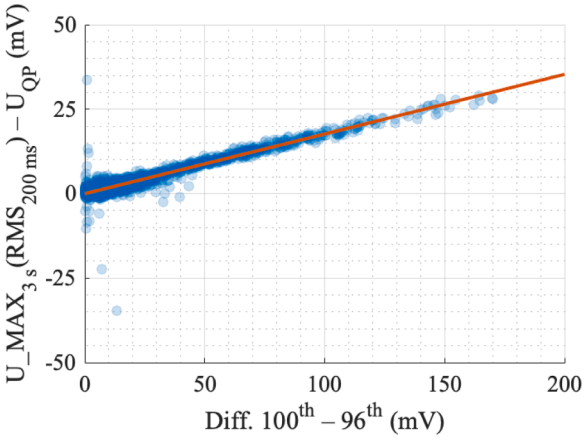

Fig. 3. Linear relationship between the outputs of the RM-A method and the CISPR 16–1–1.

As an example, Fig. 3 shows this linear relationship for one of the percentiles (100th - 96th). The graph contains the 41,595 results for each frequency band in the 2–150 kHz region, represented with blue dots, and the tendency line of the data. Results for other percentiles show also a linear relation, with a different slope. As a result, the difference between the maximum and a specific percentile can be used to characterize statistically the amplitude variability of waveforms over time; therefore, the fluctuations of the emissions are measured with this mathematical tool.

As shown in Fig. 3, the difference of QP and RMS values is linearly correlated with the difference of the percentiles, which represents the variation over time of the instantaneous RMS values. This linear relationship has been used to find a procedure to assess the QP values from the RMS spectra provided by the RM-A method.

3.4. Threshold for the QP-RMS relationship

Although different types of waveforms can be found in the electrical grid [38], a distinction can be made between the random variability over time of the background noise and the time variability of emissions

Table 1
Goodness-of-fit of the linear regressions for all percentile combinations.

Percentile combination	RMSE (mV)	Conversion factor		Percentile combination	RMSE (mV)	Conversion factor	
		a (mV)	b (mV)			a (mV)	b (mV)
$100^{th} - 99^{th}$	0.8987	0.1942	0	$100^{th} - 65^{th}$	1.0113	0.1310	0
$100^{th} - 98^{th}$	0.7532	0.1878	0	$100^{th} - 60^{th}$	1.0135	0.1308	0
$100^{th} - 97^{th}$	0.7082	0.1826	0	$100^{th} - 55^{th}$	1.0158	0.1307	0
$100^{th} - 96^{th}$	0.6915	0.1766	0	$100^{th} - 50^{th}$	1.0179	0.1305	0
$100^{t}h - 95^{th}$	0.8113	0.1617	0	$100^{th} - 45^{th}$	1.0201	0.1303	0
$100^{th} - 94^{th}$	0.9133	0.1470	0	$100^{th} - 40^{th}$	1.0222	0.1302	0
$100^{th} - 93^{rd}$	0.9228	0.1404	0	$100^{th} - 35^{th}$	1.0244	0.1300	0
$100^{th} - 92^{nd}$	0.9623	0.1362	0	$100^{th} - 30^{th}$	1.0269	0.1298	0
$100^{th} - 91^{st}$	0.9762	0.1347	0	$100^{th} - 25^{th}$	1.0300	0.1296	0
$100^{th} - 90^{th}$	0.9848	0.1339	0	$100^{th} - 20^{th}$	1.0337	0.1294	0
$100^{th} - 85^{th}$	0.9970	0.1322	0	$100^{th} - 15^{th}$	1.0379	0.1292	0
$100^{th} - 80^{th}$	1.0036	0.1316	0	$100^{th} - 10^{th}$	1.0429	0.1289	0
$100^{th} - 75^{th}$	1.0063	0.1313	0	$100^{th} - 5^{th}$	1.0515	0.1284	0
$100^{th} - 70^{th}$	1.0088	0.1312	0	$100^{th} - 0^{th}$	1.0743	0.1273	0

from different sources. In order to avoid that the random variation pattern of the background noise affects the analysis, the frequency bands whose amplitude is lower than a specific threshold level in RM-A method's maximum spectra, e.g., $U\_MAX_{3\ s}(RMS_{200\ ms})$, are discarded from the statistical analysis. This threshold level is set to 0.5637 mV, which corresponds to the 2% of the lowest CL of IEC 61,000–2–2 in the frequency range between 2 kHz and 150 kHz (see Eq. (1)). The minimum of CL in this range corresponds to 150 kHz value, whose corresponding CL limit is 89 dBμV.

$$Noise\ threshold = 2\% \cdot 10^{89\ dB\mu V/20} \cdot 10^{3} = 0.5637\ mV \quad (1)$$

4. Obtaining the empirical relationship between RMS and QP values

This section contains the results to define the empirical relationship between RMS and QP values. The work proposes the most representative percentile combination to model the amplitude variability of disturbances. Additionally, this section defines a conversion procedure to estimate the statistical QP values based on the RMS values.

Since the variation over time of the instantaneous RMS values ($Y'_{B,b}$) is related to the percentiles of the statistical distribution, the percentiles that best represent this variation for each frequency band must be found. Considering the linear correlation found between ($U\_MAX_{3s}(RMS_{200\ ms}) - U_{QP}$) and the difference of percentiles, the criterion for selecting the percentiles is the best goodness-of-fit of the tendency line, calculated as the minimum root-mean-square-error (RMSE) of the values with respect to the tendency line. The procedure for the calculation of the RMSE is shown in Eq. (2), where 'N' represents the maximum number of frequency bands available in this study, i.e., 41,595 values.

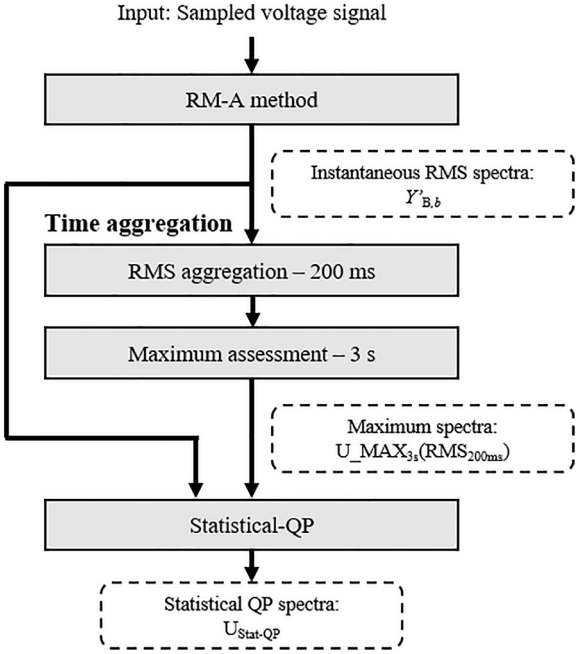

Fig. 4. Schematic overview of the Statistical-QP method.

$$RMSE = \sqrt{\frac{\sum_{i=1}^{N}(Tendency\ line_i - data_i)^2}{N}} \quad (2)$$

For this purpose, the 30 signals of the model dataset were used, and 28 combinations of percentiles were tested, in the form of ($100^{th} - X^{th}$) percentiles difference. For every ($100^{th} - X^{th}$) percentiles difference, the tendency line and the corresponding RMSE of the values are calculated. The percentile that provides the minimum RMSE was selected as the best approximation to define the linear relationship between the metrics under test. This tendency can be modeled with the Eq. (3), which represents an approximation of the differences between CISPR 16 QP values (U_{QP}) and the maximum values of RM-A method ($U\_MAX_{3s}(RMS_{200\ ms})$). The following equation can be also used as a conversion factor from RMS to QP values, where 'a' is the slope of the linear tendency line and 'b' the y-intercept.

$$Conversion\ factor = \left(100^{th} - X^{th}\right) \cdot a + b \approx U\_MAX_{3s}(RMS_{200\ ms}) - U_{QP} \quad (3)$$

For constant amplitude waveforms, without variability pattern over time, QP and the RMS values are equal [32]. Thus, for non-fluctuating waveforms the ($100^{th} - X^{th}$) percentile difference and the ($U\_MAX_{3s}(RMS_{200\ ms}) - U_{QP}$) will be 0 mV. For this reason, the tendency line is forced to pass through (0,0) and coefficient 'b' is set to zero.

Table 1 shows the results of the RMSE and the parameters of the conversion factors for the 28 combinations of percentiles. This table has been obtained after calculating the 29 percentiles required, which means that 180,938,250 instantaneous RMS values have been processed in order to obtain the 28 trend lines with their respective RMSE of the goodness-of-fit.

As shown in Table 1, the most representative percentiles difference to relate the RMS and the QP values is ($100^{th} - 96^{th}$), which provides the lowest RMSE. Fig. 3 shows the statistical distribution of this combination of percentiles, on which the corresponding conversion factor is plotted. As a result, the conversion factor calculated for all the frequency bands of the 30 signals of the model dataset that exceed the noise threshold is shown in Eq. (4).

$$\begin{aligned} Conversion\ factor &= \left(100^{th} - 96^{th}\right) \cdot 0.1766 + 0 \\ &= \left(100^{th} - 96^{th}\right) \cdot 0.1766\ (mV) \end{aligned} \quad (4)$$

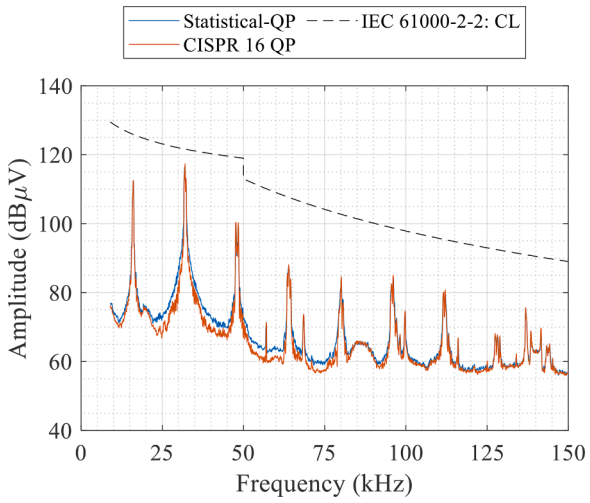

Fig. 5. Spectra obtained with Statistical-QP and CISPR 16 method for a signal measured in the POC of a PV inverter.

5. Statistical-QP: statistical method to calculate the QP values for LV grid disturbances

The empirical relationship between the RMS-QP spectra can be the basis for the estimation of QP values in RMS measuring devices. This section describes the assessment procedure of the proposed method to obtain statistical QP spectra from the outputs of RM-A method. The proposed method ('Statistical-QP' method) demands lower computational and memory requirements with respect to a QP detector, which allows obtaining QP values in simple and inexpensive RMS measuring devices. The accuracy of the QP results is also evaluated in this section.

5.1. Description of the method

The 'Statistical-QP' method is based on the use of the conversion factor that relates RMS and QP values, to obtain QP values from the RMS values provided by the RM-A method.

The Statistical-QP method is a two-stage process: firstly, the maximum amplitude of voltage levels is calculated, and then, the conversion factor is computed and its value, which depends on the variation over the time of the RMS values, is subtracted to the maximum amplitude to assess the QP values.

As shown in Fig. 4, the RM-A method provides both the instantaneous RMS spectra ($Y'_{B,b}$) and the maximum spectra ($U\_MAX_{3\ s}(RMS_{200\ ms})$). Then, the 100th and 96th percentiles of the instantaneous RMS spectra for each frequency band are calculated. The conversion factor (described in Section 4) is assessed for each frequency band, and then subtracted to the maximum values of the RM-A method, to obtain the QP values. This procedure is described in Eq. (5).

$$\begin{aligned} StatQP &= U\_MAX_{3\ s}(RMS_{200\ ms}) - Conversion\ factor \\ &= U\_MAX_{3\ s}(RMS_{200\ ms}) - \left(100^{th} - 96^{th}\right)\cdot 0.1766\ (mV) \end{aligned} \quad (5)$$

The Statistical-QP method can be used to measure voltage values for 9–150 kHz in long-term surveys, by applying the procedure to 3 s measurement intervals with a sliding window in steps of 200 ms. Thus, every 200 ms the percentiles and the maximum spectrum should be recalculated to update the conversion factor. According to the definition of the QP detector [20], the QP spectra of the long measurement is composed of the maximum value of the intermediate QP values for each frequency band.

Table 2
Relative differences of the spectra obtained with CISPR 16 and Statistical-QP methods.

Frequency band (kHz)	Relative difference of QP spectra
16.1	2.13%
32.3	2.77%
48.4	5.52%
63.5	-1.88%
80.1	9.05%
95.6	-0.33%

Table 3
Comparison of Statistical-QP and CISPR 16 outputs.

	Absol. value of diff.		Relative diff.	Relative diff. w.r.t. compatib. levels	
	Median	St. dev.	Median	Freq. bands with diff. < 2% of CL	Freq. bands with diff. < 10% of CL
All the frequency bands above noise threshold	0.002 mV	1.896 mV	7.55%	99.10%	99.95%
Frequency bands of the 50 highest values of each signal	0.075 mV	5.945 mV	5.38%	95.52%	99.51%

5.2. Accuracy analysis

This section analyses the accuracy of the proposed method. For that, the results are compared to those given by a digital implementation of the CISPR 16 standard. Fig. 5 shows the spectra computed with both methods (digital implementation of CISPR 16 and Statistical-QP) for a 3-second recording measured at the POC of a PV inverter. The results of both methods nearly overlapped for the whole 9–150 kHz band, especially at those frequencies where the disturbances present high amplitude values, and an accurate assessment is needed. This is a remarkable aspect if the purpose is the comparison of the amplitudes of the disturbances against the CL. Hence, the relative differences between the spectra for the highest amplitudes of the signal are lower than 10%, as shown in Table 2.

In order to evaluate the accuracy of the empirical RMS-QP relationship obtained in this work, a comprehensive accuracy study of its use for QP assessment has been developed. For that purpose, the proposed method and the digital implementation of the CISPR 16 method have been applied to a set of recordings in the LV distribution grid. Then, the differences in the results between both methods have been statistically analyzed for all the frequency bands exceeding the noise threshold stated in section 3.4.The statistical analysis evaluates the absolute differences, in terms of the median value and the standard deviation, and the relative differences, in terms of the median value and the comparison against the 2% and 10% of the CL (see Table 3). This last aspect allows the evaluation of the results with respect to a known and standardized reference level. The statistical study has been applied to the remaining 29 recordings of the validation dataset that were not used on the definition of the conversion factor.

As one of the main applications of this method is the measurement of high amplitude disturbances in the grid, a complementary evaluation of the proposed method has been carried out: the 50 frequency bands with the highest amplitudes of each recording have been identified and compared to the CISPR 16 outputs. A similar statistical analysis has been applied to these high-amplitude values, as it can be seen in Table 3.

The analysis shows that the Statistical-QP method provides results very similar to the digital implementation of CISPR 16. The absolute differences are within few millivolts for the whole 9–150 kHz band (see Table 3) and the median relative difference is below 10%, which is a typical uncertainty value for PQ instruments. Moreover, 99.10% of the

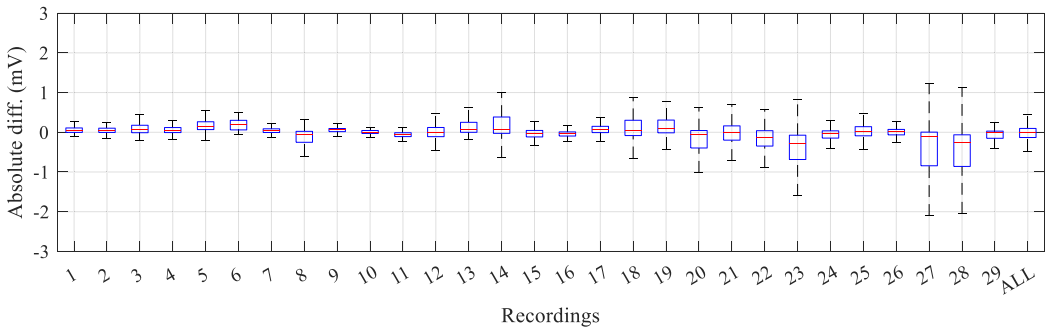

Fig. 6. Boxplot representing the absolute values of the differences between the RMS spectra of IEC 61,000–4–7 and the proposed method.

Table 4
Computational requirements of Statistical-QP and CISPR 16 methods.

Method	Time step	Number of FFT	Memory (QP output)	Memory (spectrogram)	Elapsed real time	CPU processing time
CISPR 16	2 ms	1491	0.68 MB	203.23 MB	6.60 s	9.83 s
Statistical-QP	20 ms	150	1.77 MB	1.77 MB	0.39 s	0.57 s

frequency bands provide a difference lower than 2% of the CL and the 99.95% of them are lower than 10% of the CL.

Regarding the evaluation of the 50 highest amplitudes of each recording, the results are similar: the median of the relative differences is close to 5%, and the 95.52% of the frequency bands provide a difference lower than 2% of the CL and the 99.51% lower than 10%.

The absolute values of the differences between the outputs of CISPR 16 and Statistical-QP are shown in Fig. 6, where the boxes represent the values between 25% and 75% and the whiskers represent 95% of the values. It can be observed that the Stat-QP method provides accurate values, as 95% of the differences are within a few millivolts for the individual recordings and below +/- 1 mV for the whole set of recordings.

In conclusion, the Statistical-QP method, which is a direct application of the empirical relationship between the RMS and QP spectra obtained in this work, provides QP values comparable to the CISPR 16 standard method. Similar accuracy is obtained when only the highest amplitude disturbances are considered. Therefore, the proposed method can be applicable for the comparison of grid disturbances against CL with simple and fast calculations, without the need of implementing a QP detector.

5.3. Evaluation of computational and memory requirements

The evaluation of the computational and memory requirements of the proposed method is a key aspect to evaluate its applicability to massive deployments of simple and inexpensive PQ measurement instruments to measure the amplitude of disturbances in the supraharmonic frequency range. This section analyzes and compares the memory and computational resources needed for the implementation of the CISPR 16 and Statistical-QP methods.

The study has been performed under the same test bed (MacBook Pro, CPU 2.6 GHz Intel Core i5 dual core, RAM 8 GB 1600 MHz DDR3 and Matlab R2019b) with a 3-second voltage recording measured in the LV grid. The results, summarized in Table 4, show that the Statistical-QP method requires 10 times less computational resources, due to the reduced number of FFT's. Moreover, the execution time ('Elapsed real time' and 'CPU processing time' in Table 4) of the proposed method is more than 15 times less than the CISPR 16 method. Lastly, although the Statistical-QP method requires 3 times more memory resources to obtain the QP output (the data needed to calculate the percentiles must be saved), the novel method requires 100 times lower storage resources to obtain a spectrogram of 3 s length.

6. Conclusions

Currently, there is not a normative framework to measure supraharmonic disturbances in the LV grid. The Annex C of IEC 61,000–4–30 standard proposes three measurement methods to characterize voltage values in the 9–150 kHz range. Nonetheless, this annex is classified as 'informative'; hence, PQ instrument manufacturers and utilities are not obligated to implement or use the methods described in the IEC 61,000–4–30. The RMS spectra are the most common metrics used in PQ instruments to measure voltage values of supraharmonic disturbances. Nonetheless, the CL regulated in IEC 61,000–2–2 for disturbances propagated through the LV grid are defined in terms of QP values. As there is no relation between the QP and RMS spectra, it will be useful to count on a simple procedure to assess the QP values with RMS measuring devices. The definition of a relationship between RMS and QP values could be beneficial to develop PQ instruments that provide RMS and QP values with simpler calculations, less computational resources and without implementing a QP detector. Furthermore, the RMS-QP relationship could be used as a first assessment of CL compliance with existing PQ devices.

This paper proposes a methodology that empirically relates the RMS and QP voltage values in the 9–150 kHz region, which has been developed from recordings measured in the LV grid. This relationship uses the outputs of the CISPR 16 standard method and the RM-A method to link statistically the amplitude variations of voltage values with respect to the differences between the RMS and QP spectra. In addition, the most representative statistic to model the differences of the results of both voltage metrics is identified. Furthermore, a conversion factor to estimate the QP spectra from maximum RMS values is proposed.

Additionally, in this work a statistical measurement method (labeled as 'Statistical-QP') is developed which is an application of the proposed empirical relationship between QP-RMS spectra. The comparison of the outputs of both methods, performed with recordings from the LV grid not used in the definition of the relationship, shows that the amplitude values obtained with the novel method are comparable to the CISPR 16 QP spectra. Nevertheless, the computational burden and the memory requirements needed for the execution of the Statistical-QP are significantly lower than for the CISPR 16.

The Statistical-QP method was presented to IEC SC77A/WG9 and discussed as a tentative measurement method in a new edition of the IEC 61,000–4–30 standard.

CRediT authorship contribution statement

Alexander Gallarreta: Conceptualization, Methodology, Software, Investigation, Writing – original draft. **Igor Fernández:** Formal analysis, Investigation. **Deborah Ritzmann:** Formal analysis, Writing – original draft. **Stefano Lodetti:** Investigation, Writing – review & editing. **Victor Khokhlov:** Validation. **David de la Vega:** Conceptualization, Methodology, Supervision, Writing – review & editing. **Paul Wright:** Project administration, Funding acquisition. **Jan Meyer:** Supervision.

Declaration of Competing Interest

The authors declare that they have no known competing financial interests or personal relationships that could have appeared to influence the work reported in this paper.

Data availability

The data that has been used is confidential.

Acknowledgements

This project (18NRM05) has received funding from the EMPIR program co-financed by the Participating States and from the European Union's Horizon 2020 research and innovation program. This work was funded in part by the Basque Government under the grants IT1436–22 and PRE_2022_2_0074. This work was supported in part through grant PID2021–124706OB-I00 funded by MCIN/AEI/10.13039/501100011033 and by ERDF A way of making Europe.

References

[1] M.H.J. Bollen, et al., Power quality concerns in implementing smart distribution-grid applications, IEEE Trans. Smart Grid Vol. 8 (2017), https://doi.org/10.1109/TSG.2016.2596788.
[2] S.K. Rönnberg, M.H.J. Bollen, H. Amaris, G.W. Chang, I.Y.H. Gu, Ł.H. Kocewiak, J. Meyer, M. Olofsson, P.F. Ribeiro, J. Desmet, On waveform distortion in the frequency range of 2 kHz–150 kHz—review and research challenges, Electric. Power Syst. Res. Vol. 150 (2017), https://doi.org/10.1016/j.epsr.2017.04.032.
[3] I. Fernández, D. de la Vega, A. Arrinda, I. Angulo, N. Uribe-Pérez, A. Llano, Field trials for the characterization of non-intentional emissions at low-voltage grid in the frequency range assigned to NB-PLC technologies", Electronics (Basel) 8 (2019) https://doi.org/10.3390/electronics8091044.
[4] S.T.Y. Alfalahi, et al., Supraharmonics in power grid: identification, standards, and measurement techniques, IEEE Access 9 (2021), https://doi.org/10.1109/ACCESS.2021.3099013.
[5] J. Sutaria, S. Rönnberg, A. Espín-Delgado, Analysis of supraharmonics in a three-phase frame, Electric. Power Syst. Res. 203 (2022), https://doi.org/10.1016/j.epsr.2021.107668.
[6] PD CLC/TR 50627:2015, Study report on electromagnetic interference between electrical equipment /systems in the frequency range below 150 kHz, 2015. http://standardsproposals.bsigroup.com/Home/getPDF/2326.
[7] PD CLC /TR 50669 : 2017, Investigation Results on Electromagnetic Interference in the Frequency Range below 150kHz, 2017.
[8] A. Abart, G.F. Bartak, EMI of emissions in the frequency range 2kHz - 150 kHz, in: 22nd International Conference and Exhibition on Electricity Distribution (CIRED 2013), Stockholm, 2013, https://doi.org/10.1049/cp.2013.1151.
[9] V. Khokhlov, J. Meyer, P. Schegner, D. Agudelo-martinez, A. Pavas, Immunity assessment of household appliances in the frequency range from 2 to 150 kHz, in: 25th International Conference on Electricity Distribution (CIRED), Madrid, 2019, https://doi.org/10.34890/283.
[10] S. Sakar, S. Ronnberg, M. Bollen, Interferences in AC–DC LED drivers exposed to voltage disturbances in the frequency range 2–150 kHz, IEEE Trans. Power Electron. 34 (2019), https://doi.org/10.1109/TPEL.2019.2899176.
[11] A. Espín-Delgado, S. Rönnberg, S. Sudha Letha, M. Bollen, Diagnosis of supraharmonics-related problems based on the effects on electrical equipment, Electric Power Syst. Res. 195 (2021), https://doi.org/10.1016/j.epsr.2021.107179.
[12] P.M. Körner, R. Stiegler, J. Meyer, T. Wohlfahrt, C. Waniek, J.M.A. Myrzik, Acoustic noise of massmarket equipment caused by supraharmonics in the frequency range 2 to 20 kHz, in: 2018 18th International Conference on Harmonics and Quality of Power (ICHQP), Ljubljana, Slovenia, 2018, https://doi.org/10.1109/ICHQP.2018.8378856.
[13] V. Ravindran, S. Sakar, Sarah Rönnberg, M.H.J. Bollen, Characterization of the impact of PV and EV induced voltage variations on LED lamps in a low voltage installation, Electric Power Syst. Res. 185 (2020), https://doi.org/10.1016/j.epsr.2020.106352.
[14] M. Wasowski, et al., Sources of non-intentional Supraharmonics in LV network and its impact on OSGP PLC communication – experimental study, IEEE Trans. Power Delivery 37 (2022), https://doi.org/10.1109/TPWRD.2022.3175090.
[15] Electromagnetic compatibility (EMC) - Environment - Compatibility levels for low-frequency conducted disturbances and signalling in public low-voltage power supply systems, IEC 61000-2-2:2002+A2:2019 Ed. 2.2, 2002.
[16] Electromagnetic compatibility (EMC) - Part 4-19: testing and measurement techniques - test for immunity to conducted, differential mode disturbances and signalling in the frequency range, IEC 61000-4-19:2014 Ed. 1.0, 2014.
[17] Electromagnetic compatibility (EMC) - Part 4-30: testing and measurement techniques - power quality measurement methods, IEC 61000-4-30:2015 Ed. 3.0, 2015.
[18] International electrotechnical vocabulary - Part 151: electrical and magnetic devices, IEC (2019), 60050-151:2001/AMD3:2019.
[19] Electromagnetic compatibility (EMC) - Part 4-7: testing and measurement techniques - General guide on harmonics and interharmonics measurements and instrumentation, for power supply systems and equipment connected thereto, IEC 61000-4-7:2002+A1:2009 Ed. 2.1, 2002.
[20] Specification for radio disturbance and immunity measuring apparatus and methods - Part 1-1: radio disturbance and immunity measuring apparatus - Measuring apparatus, CISPR 16-1-1:2019, 2019.
[21] Specification for radio disturbance and immunity measuring apparatus and methods - Part 3: CISPR technical reports, PD CISPR/TR 16-3:2010+A1:2012, 2015.
[22] A. Gallarreta, I. Fernández, D. Ritzmann, S. Lodetti, V. Khokhlov, P. Wright, J. Meyer, D. de la Vega, A light measurement method for 9-150kHz disturbances in power grids comparable to CISPR Quasi-Peak, IEEE Trans. Instrum. Meas. (2022), https://doi.org/10.1109/TIM.2022.3195255.
[23] S. Lodetti, A. Gallarreta, D. Ritzmann, V. Khokhlov, P. Wright, J. Meyer, I. Fernández, D. de la Vega, On the suitability of the CISPR 16 method for measuring conducted emissions in the 2–150kHz range in low voltage grids", Electric. Power Syst. Res. 216 (2023) https://doi.org/10.1016/j.epsr.2022.109011.
[24] V. Khokhlov, J. Meyer, P. Schegner, Thermal interactions in modern lighting equipment due to disturbances in the frequency range 2–150 kHz", in: 2019 IEEE Milan PowerTech, Milan, 2019, https://doi.org/10.1109/PTC.2019.8810460.
[25] D. Darmawardana, S. Perera, D. Robinson, J. David, J. Meyer, U. Jayatunga, Impact of high frequency emissions (2–150kHz) on lifetime degradation of electrolytic capacitors in grid connected equipment, in: 2019 IEEE Power & Energy Society General Meeting (PESGM), Atlanta, 2019, https://doi.org/10.1109/PESGM40551.2019.8973849.
[26] S. Lodetti, J. Bruna, J.J. Melero, V. Khokhlov, J. Meyer, A Robust wavelet-based hybrid method for the simultaneous measurement of harmonic and supraharmonic distortion, IEEE Trans. Instrum. Meas. 69 (2020), https://doi.org/10.1109/TIM.2020.2981987.
[27] S. Zhuang, W. Zhao, Q. Wang, Z. Wang, L. Chen, S. Huang, A high-resolution algorithm for supraharmonic analysis based on multiple measurement vectors and Bayesian compressive sensing, Energies 12 (2019), https://doi.org/10.3390/en12132559.
[28] S. Zhuang, W. Zhao, R. Wang, Q. Wang, S. Huang, New measurement algorithm for supraharmonics based on multiple measurement vectors model and orthogonal matching pursuit, IEEE Trans. Instrum. Meas. 68 (2019), https://doi.org/10.1109/TIM.2018.2878613.
[29] G. Frigo, Measurement of conducted supraharmonic emissions: quasi-peak detection and filter bandwidth, Metrology 2 (2022), https://doi.org/10.3390/metrology2020011.
[30] T.M. Mendes, D.D. Ferreira, L.R.M. Silva, P.F. Ribeiro, J. Meyer, C.A. Duque, PLL based method for supraharmonics emission assessment, IEEE Tran. Power Delivery 37 (2022), https://doi.org/10.1109/TPWRD.2021.3112404.
[31] T.M. Mendes, C.A. Duque, L.R.M. Silva, D.D. Ferreira, J. Meyer, Supraharmonic analysis by filter bank and compressive sensing, Electric Power Syst. Res. 169 (2019), https://doi.org/10.1016/j.epsr.2018.12.016.
[32] D. Ritzmann, S. Lodetti, D. De La Vega, V. Khokhlov, A. Gallarreta, P. Wright, J. Meyer, I. Fernandez, D. Klingbeil, Comparison of measurement methods for 2-150kHz conducted emissions in power networks, IEEE Trans Instrum Meas 70 (2020), https://doi.org/10.1109/TIM.2020.3039302.
[33] T.M. Mendes, et al., Comparative analysis of the measurement methods for the supraharmonic range, Int. J. Electric. Power & Energy Syst. 118 (2020), https://doi.org/10.1016/j.ijepes.2019.105801.
[34] V. Khokhlov, J. Meyer, A. Grevener, T. Busatto, S.K. Ronnberg, Comparison of measurement methods for the frequency range 2-150kHz (Supraharmonics) based on the present standards framework, IEEE Access Vol.8 (2020), https://doi.org/10.1109/ACCESS.2020.2987996.
[35] A. Gallarreta, I. Fernández, D. Ritzmann, S. Lodetti, V. Khokhlov, P. Wright, J. Meyer, D. de la Vega, Adaptation of the IEC 61000-4-7 measurement method to CISPR Band A (9-150kHz)", in: 2022 IEEE 12th International Workshop on Applied Measurements for Power Systems, Cagliari, Italy, 2022, https://doi.org/10.1109/AMPS55790.2022.9978818.
[36] I. Fernández, M. Alberro, J. Montalbán, A. Arrinda, I. Angulo, D. de la Vega, A new voltage probe with improved performance at the 10 kHz–500kHz frequency range

for field measurements in LV networks, Measurement 145 (2019), https://doi.org/10.1016/j.measurement.2019.05.106.

[37] M. Klatt, J. Meyer, P. Schegner, R. Wolf, B. Wittenberg, Filter for the measurement of supraharmonics in public low voltage networks, in: 2015 IEEE International Symposium on Electromagnetic Compatibility, Dresden, Germany, 2015, https://doi.org/10.1109/ISEMC.2015.7256141.

[38] I. Fernandez, N. Uribe-Pérez, I. Eizmendi, I. Angulo, D. de la Vega, A. Arrinda, T. Arzuaga, Characterization of non-intentional emissions from distributed energy resources up to 500 kHz: a case study in Spain, Int. J. Electric. Power & Energy Syst. 105 (2019), https://doi.org/10.1016/j.ijepes.2018.08.048.